Guided Wave Based Identification of In-Plane Fibre Waviness Defect in A Honeycomb Composite Sandwich Structure Using Antisymmetric Modes

Abdul Latheef Thalapil
Department of Mechanical Engineering
Sarabhai Institute of Science and Technology Trivandrum, KL, India
doi.org/10.64643/IJIRTV12I10-204360-459

***Abstract*—Waviness is a common geometrical defect in carbon fiber reinforced plastics (CFRP) plates, characterized by local misalignment of an otherwise region of straight fibers. Presence of fiber waviness is a potential source of non-linearity and affects the relative strength of the composite structure. Recently, guided wave (GW) based in situ NDE techniques have been extensively used for damage detection in composite laminates, albeit for damages other than fiber waviness. This study explores the feasibility of using ultrasonic guided waves to characterize in- plane fiber waviness in honeycomb composite sandwich structures (HCSS). In-plane fiber waviness, a process-induced defect in carbon fibre reinforced plastics (CFRP), introduces ply ripples that degrade structural strength. While guided wave methods are well established for detecting defects like delamination and disbond, their application for waviness characterization remains unexplored. The anti-symmetric *A*0 mode is employed to numerically investigate the influence of in-plane fiber waviness on guided wave propagation using the *Curvilinear physics* framework in a commercially available finite element (FE) modeling pack- age (COMSOL Multiphysics). Results show that in-plane fiber waviness causes a detectable phase shift in *A*0 mode, enabling localization within a network of PZT sensors by utilizing damage index (DI) mapping algorithm. The efficacy of the method is demonstrated using noise-augmented FE generated GW data set for an HCSS panel.**

***Index Terms*—Fibre waviness; ultrasonic guided wave; non- destructive testing; honeycomb composite sandwich structure (HCSS)**

I. INTRODUCTION

Honeycomb composite sandwich structures (HCSS), comprising a lightweight honeycomb core bonded to carbon fibre (graphite/epoxy) face sheets, are extensively employed in aerospace, automotive, marine, and defense systems owing to their excellent strength-to-weight ratio and high stiffness [1]. Their structural response can be tailored by modifying the core architecture as well as the material and thickness of the face sheets [1]. However, the complexity of their manufacturing routes renders HCSS susceptible to defects such as matrix cracking, debonding, delamination, fibre waviness, and local yielding [2]. These fabrication-induced imperfections can modify the effective material behavior and may serve as initiation sites for damage under operational loading. Consequently, establishing appropriate manufacturing quality criteria and acceptable defect limits is essential to balance structural safety against production cost [3].

Fibre waviness is a geometric imperfection in which fibres deviate locally from their intended design orientation. In carbon fibre reinforced plastics (CFRP), such waviness typically develops during manufacturing stages including draping, resin infiltration, and curing. Depending on the direction of misalignment, fibre waviness is generally categorized as in- plane or out-of-plane. Previous studies have shown that fibre waviness degrades the tensile and compressive performance of composite laminates [4], [5], with larger fibre shear angles producing more pronounced reductions in stiffness and strength. Under service conditions, these defects can evolve into critical structural damage. Because repair of affected regions is often challenging and expensive, reliable non-destructive evaluation (NDE) of fibre waviness is crucial for maintaining the integrity and quality of composite structures [6].

A variety of NDT&E techniques are employed for assessing aerospace composite components, including

ultrasonic testing (UT), guided-wave (GW) methods, eddy current testing (ET), X-ray computed tomography (X-ray CT), and thermography [7]– [11]. Among these, X-ray CT, ET, and UT have been applied to the detection of fibre waviness [12]–[14]. ET is predominantly sensitive to near-surface anomalies, whereas X- ray CT involves radiation-safety issues and limited accessibility, which can restrict its field use [15]. Owing to its high penetration capability and sensitivity to internal discontinuities, UT is widely adopted for in-situ inspection of aerospace composites [16], [17]. Nevertheless, fibre waviness tends to generate weak ultrasonic echo signals, making it difficult to detect, and conventional UT typically requires immersion or couplants to ensure efficient acoustic coupling [18].

Due to the anisotropic nature and often complex geometries of composite structures, ultrasonic guided-wave (GW)-based NDT&E provides strong capabilities for damage detection and localization, even in the presence of data loss or environmental variability [19], [20]. Guided waves have been extensively demonstrated as effective tools for assessing structural integrity in composite components. In sandwich architectures, fibre waviness has been shown to induce localized stiffness reductions, which in turn decrease the group velocity of certain GW modes [21].

In this work, a guided-wave (GW)–based NDT&E frame- work is developed to detect in-plane fibre waviness in honey- comb composite sandwich structures (HCSS) using numerical simulation. Out-of-plane excitation is employed to preferentially generate the fundamental antisymmetric (A_0) mode, and its interaction with fibre waviness is analyzed through finite element (FE) modeling. Fibre waviness is represented via a curvilinear-physics formulation that captures in-plane deviations of the fibre paths within individual plies. The use of out-of-plane actuation reduces interfacial stress concentrations and mitigates the risk of disbonding that is often associated with conventional in-plane PZT excitation. In practical implementations, such loading can be realized using acoustic emission (AE)–type contact sensors. The numerical results indicate that local stiffness degradation caused by in-plane waviness lowers the (A_0)-mode group velocity, producing a measurable phase shift that can be used as a robust damage indicator under noise-contaminated conditions.

II. METHODOLOGY

A. Analytical formulation of in-plane fibre waviness

In-plane fibre waviness refers to deviations of fibres within an individual ply from their nominal straight alignment, typically caused by lateral fibre shifting during lay-up. The severity of waviness is commonly quantified using the severity factor $\alpha = \frac{A}{L}$, defined as ratio of amplitude of waviness (A) to length (L) (Figure 1), and is widely used to assess its influence on the mechanical behaviour of CFRP laminates [22], [23]. Hsaio and Daniel investigated the corresponding reduction in elastic stiffness by modelling the waviness as a planar sinusoidal perturbation [24]. Building on this analytical approach, this section examines the influence of uniform in-plane waviness on the stiffness of the composite skin.

The waviness is assumed to be planar sinusoidal as shown in Figure 1 of the form:

$$v = A \sin\left(\frac{2\pi x}{L}\right) \quad (1)$$

where v is the displacement component along the y direction. Detailed expressions for elements of the effective compliance matrix, Sij, are functions of the severity factor α [?], and are omitted for brevity. The stiffness matrix Dij can be obtained as:

$$D_{ii} = S_{ii}^{-1} \quad (2)$$

B. Structure

The influence of in-plane fiber waviness on the elastic stiffness of the composite skin was investigated by analyzing a 14.97 mm thick HCSS panel. The panel consists of a 12.7 mm thick aluminum honeycomb core bonded on both faces via a 0.01 mm thick adhesive layer to a 1.125 mm thick CFRP face sheet. The constituent material properties are summarized in Table I. In-plane fibre waviness defects can occur in top or bottom CFRP skin. Using these material properties, the effective stiffness values *Dii* of an individual CFRP lamina affected with in-plane waviness were calculated for increasing values of α (Figure 2).

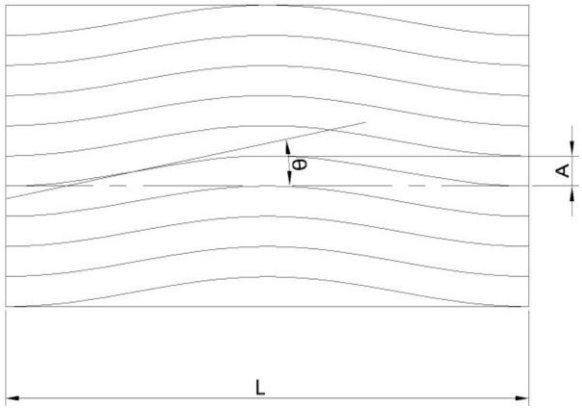

Fig. 1. Representative volume element and coordinates for sandwich composite structure with in-plane fiber waviness in *xy* plane.

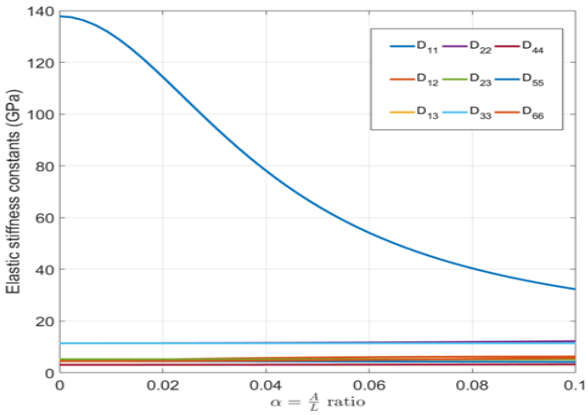

Fig. 2. Variation of elastic stiffness constants of individual CFRP lamina with increasing severity factor α.

C. FE modeling of fibre waviness & simulation setup

In order to evaluate the effect of in-plane fibre waviness on GW propagation, 3D numerical FE simulations were per- formed using COMSOL Multiphysics 6.3. Considering the computational complexity, a model of dimensions 150 mm × 200 mm × 14.97 mm with an in-plane fibre waviness of size 50 mm × 50 mm as shown in Figure 3 was analyzed, and the arrangement of transducers was chosen as shown in Figure 4. Out-of-plane loading in the *z*-direction was applied at the transducer locations to excite the A_0 Lamb wave mode in the panel. The material properties of the panel were defined using the *Structural Mechanics* module in COMSOL Multiphysics

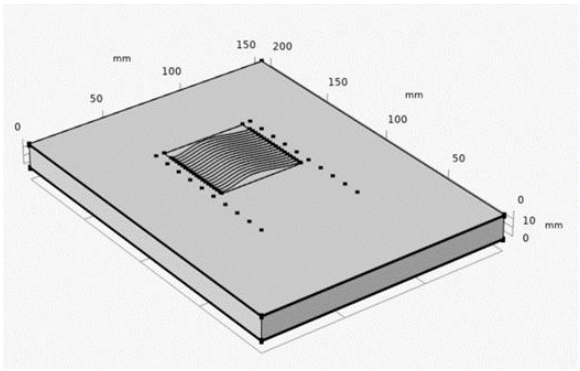

Fig. 3. Finite element 14.97 mm thick HCSS plate model with network of ten transducer paths with in-plane fiber waviness of size 50 mm × 50 mm.

TABLE I Material properties (standard notations) of CFRP lamina used in facesheet, adhesive and honeycomb core in HCSS

Material	$E11$(GPa)	$E22$(GPa)	$E33$(GPa)	$G12$(GPa)	$G23$(GPa)	$G13$(GPa)	$v12$	$v13$	$v23$	ρ(kg/m^3)
CFRP lamina	135	9	9	4.5	3.103	4.5	0.29	0.29	0.45	1780
Adhesive	4.35	4.35	4.35	1.599	1.599	1.599	0.36	0.36	0.36	1100
Honeycomb core	0.028	0.028	0.40	0.074	0.103	0.221	0.318	3.18×10^{-5}	3.18×10^{-5}	36.8

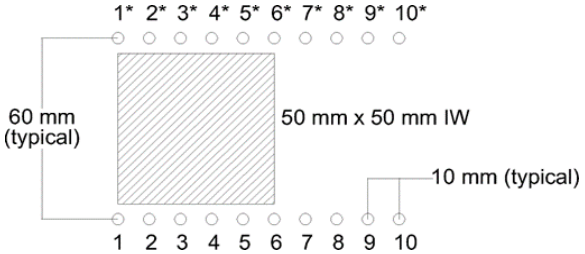

Fig. 4. Top view of ten transducer paths on the sandwich panel used for FE simulations.

6.3. In-plane fibre waviness was incorporated through the *Curvilinear Coordinates* interface, which enabled the creation of a curvilinear coordinate system to assign anisotropic mate- rial properties aligned with the waviness pattern of the region. The analysis was performed using a *Time-Implicit* study. The mesh size and time-step increment in the *Time-Implicit* analysis significantly influence the accuracy of finite element (FE) simulation results [25]. Previous studies

on FE simulation of Lamb wave propagation suggest that the maximum element size should be smaller than one-sixth of the wavelength of the propagating mode [26]. For an excitation frequency of f = 100 kHz, the wavelength of the A_0 mode in the HCSS panel was approximately 14.35 mm, estimated from the group velocity obtained from the dispersion curve shown in Fig. 5. Accordingly, the maximum mesh size in the plate was limited to 2 mm, and a *Swept* mesh was employed for the adhesive layer.

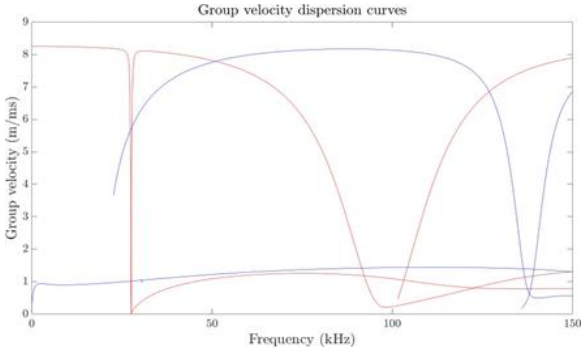

Fig. 5. Group velocity dispersion curves for 14.97 mm thick HCSS composite panel using Dispersion Calculator

The time-step size was selected as 0.1 µs ($> 1/60f$). The time-domain profile of the applied out-of-plane point load was defined as a five-cycle sinusoidal pulse modulated by a Hanning window and expressed as:

$$V(t) = 0.5\left[1 - \cos\left(\frac{2\pi ft}{5}\right)\right]\sin(2\pi ft) \quad (3)$$

Time-domain FE simulations were performed to obtain signal responses for ten transmitter–receiver paths, denoted $P_{x\text{-}x}*$, where transducer x acts as the transmitter and transducer x^* as the receiver, for x = 1, 2, . . ., 10, corresponding to the sensor layout depicted in Fig. 4. Each time-series record spanned a duration of 100 µs at a sampling rate of 10 MHz. The discretized model comprised 485,550 elements and 2,842,344 degrees of freedom. The average computation time per propagation path was 120 h. All simulations corresponding to the seven propagation paths were performed on a 64-bit workstation equipped with an Intel® Core™ i7-7700HQ processor operating at 2.80 GHz and 32 GB of RAM.

Practical guided wave (GW) data acquisition systems generally exhibit signal-to-noise ratio (SNR) values in the range of 20 dB to 50 dB [28], [29]. In addition to inherent measurement noise, signal quality can be further affected by variations in operational and environmental conditions [30], [31]. To emulate these realistic measurement uncertainties within the simulation framework, both additive white noise and pink noise were introduced to the FE-generated GW signals, resulting in a combined SNR of 20 dB. The noise-contaminated signal is given by:

$$s_n(t) = s(t) + \beta \max|s(t)|[w(t) + p(t)] \quad (4)$$

where $s_n(t)$ and $s(t)$ represent the noisy and noise-free signals, respectively; max($s(t)$) denotes the peak amplitude of $s(t)$; β = 0.0275 is a scaling coefficient that controls the noise level; and $w(t)$ and $p(t)$ correspond to white and pink noise sequences, respectively, each generated independently from a zero-mean Gaussian distribution with unit standard deviation.

The impact of in-plane fibre waviness in the top CFRP skin was studied using this noise augmented data set.

III. SIGNAL DIFFERENCE COEFFICIENT BASED DAMAGE IDENTIFICATION & LOCALIZATION

Damage identification was carried out using the conventional Signal Difference Coefficient (SDC)-based algorithm [27], a concise description of which is provided in this section. Consider a sensor network comprising N piezoelectric transducers. Let S_d denote the signal recorded at receiver i^* when transducer i operates as the transmitter, and let S_b denote the corresponding baseline signal acquired from the intact structure. The parameter t0 denotes the arrival time of the A_0 Lamb wave mode, and t_{BW} denotes the temporal duration of the window enclosing the wave packet, i.e., the temporal bandwidth of the A_0 mode. The exit time of the A_0 wave packet is accordingly defined as $t_1 = t_0 + t_{BW}$. Estimation of t_0 requires knowledge of the group velocity of the A_0 mode along the transmitter–receiver propagation path.

The SDC value associated with sensing path $P_{i\text{-}i}*$ quantifies the discrepancy between the received signal S_d and the baseline signal S_b, and is expressed in terms of the correlation coefficient deviation (CCD) as:

$$\mathrm{SDC}(i, i^*) = 1 - \mathrm{CC}(i, i^*) \quad (5)$$

Where,

$$\mathrm{CC}(i, i^*) = \frac{\sum_{t=t_0}^{t_1}(S_b(t) - \mu_b)(S_d(t) - \mu_d)}{\sqrt{\sum_{t=t_0}^{t_1}(S_b(t) - \mu_b)^2} \cdot \sqrt{\sum_{t=t_0}^{t_1}(S_d(t) - \mu_d)^2}} \quad (6)$$

Here, μ_b and μ_d denote the mean values of the time-series samples of S_b and S_d, respectively. A high degree of correlation between S_b and S_d, reflected by a large value of CC (i, i^*), indicates negligible signal alteration and implies the absence of structural damage, yielding a correspondingly low SDC value. The time of arrival (t_0) and exit (t_1) of $A0$ mode for all sensor paths for FE simulated data were observed to be 49.9 µs and 99.9 µs, respectively, corresponding to group velocity of 1.4 km/s.

For the sensor configuration shown in Fig. 4, the coordinates (x_i, y_i) and (x_j, y_j) denote the Cartesian positions of transmitter i and receiver j, respectively, with $d_{(i,j)}$ representing the straight-line distance between them. The panel inspection region is discretized into a two-dimensional grid. At each grid point (x, y), the pixel intensity of the damage index (DI) map is computed by weighting an elliptical spatial distribution function $A_{i,j}(x, y)$—whose foci coincide with the transmitter and receiver positions—by the corresponding SDC value:

$$DI(x, y) = \sum_{i=1}^{N-1} \sum_{j=i+1}^{N} \mathrm{SDC}(i, j) \cdot \frac{\beta_s - A_{ij}(x, y)}{\beta_s - 1} \quad (7)$$

where β_S is an empirically selected scaling parameter independent of the wave propagation velocity. The spatial weighting function $A_{i,j}(x, y)$ defines a non-negative elliptical contour distribution given by:

$$A_{ij}(x, y) = \begin{cases} P_{ij}(x, y), & P_{ij}(x, y) < \beta_S, \\ \beta_S, & P_{ij}(x, y) \geq \beta_S, \end{cases} \quad (8)$$

Where,

$$P_{ij}(x, y) = \frac{\sqrt{(x - x_i)^2 + (y - y_i)^2} + \sqrt{(x - x_j)^2 + (y - y_j)^2}}{d_{ij}} \quad (9)$$

The final DI map is constructed by superimposing the elliptical contributions $A_{i,j}(x, y)$ from all transmitter–receiver paths. Sensing paths that intersect a damaged region exhibit elevated SDC values, which manifest as regions of increased pixel intensity in the DI map, thereby indicating probable damage locations. Localization accuracy improves when a pronounced contrast exists between the SDC values of damaged and undamaged paths. For consistent inter-case comparison, the computed values DI (x, y) are normalized to the range $[0, 1]$.

IV. RESULTS AND DISCUSSION

In-plane fibre waviness defects reduce the mechanical rigidity of HCSS panels and induce a change in the group velocity of the A_0 Lamb wave mode propagating through the affected region, thereby introducing a phase shift in the received signal. This characteristic can be exploited for damage identification and localization within a GW-SHM framework. To demonstrate the efficacy of this method, the algorithm was tested through FE simulations for the structure shown in Figure 4, wherein the 50 mm × 50 mm region with in-plane fibre waviness defect spans the area covered by six sensor paths in the network (P1-1*, P2-2*, . . ., P6-6*). The other four paths (P7-7*, P8-8*, P9-9* and P10-10*) do not contain any defect in line of sight. The waviness defect was limited to the top skin in the simulations. To illustrate the DI mapping procedure, guided wave data are generated via FE simulations augmented with white and pink noise at a signal-to-noise ratio (SNR) of 20 dB. Discrete wavelet transforms (DWT) based denoising was applied to preprocess the guided wave (GW) signals before calculating the SDC values. A comprehensive description of the DWT-based denoising procedure is provided in the work of Rizzo *et al.* [32]. Figure 6 illustrates DWT based denoised signal for sensor path P88. DWT based pre-processing could easily be implemented in practical SHM systems, however it does not entirely get rid of the noise in the signal as seen in Figure 6.

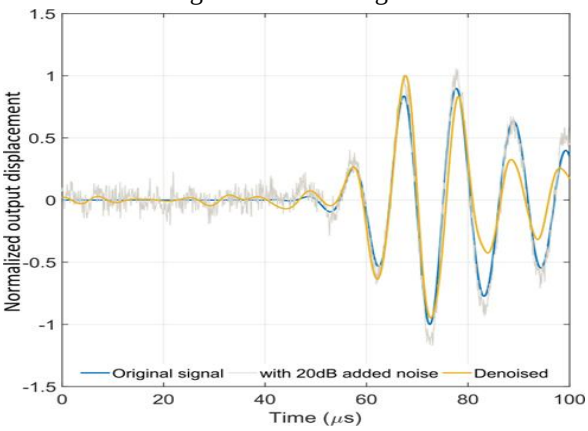

Fig. 6. Denoising of noisy signal using DWT for GW signal corresponding to sensor path P88

It is observed that SDC values for paths containing the defect in line of sight are higher than those for paths that do not contain the defect in line of sight as shown in Figure 7. The value of SDC coefficients were observed to be significantly higher (> 6%) for in-plane fibre waviness located in the top layer. Figure 7 shows that the damage is identified correctly for the 50 x 50 mm size region for uniform in-plane fiber waviness cases.

V. CONCLUSIONS

In-plane fibre waviness is a manufacturing-related defect that can substantially reduce the stiffness and load-carrying capability of honeycomb composite sandwich structures. Consequently, the development of reliable and efficient NDT&E techniques for detecting such defects is of considerable practical importance. In this study, a guided wave (GW)-based inspection approach utilizing the A_0 Lamb wave mode was proposed and evaluated for the detection and localization of in-plane fibre waviness defects in HCSS panels.

Finite element simulations were performed in COMSOL Multiphysics, where a curvilinear coordinate formulation was employed to represent the anisotropic wave propagation be- haviour associated with fibre waviness in the CFRP face sheets. To reflect signal degradation commonly observed in practical GW-based SHM systems due to operational variability, additive white and pink noise were introduced into the FE-generated signals, resulting in an overall SNR of 20 dB. Damage localization was carried out using an SDC- based damage index (DI) mapping algorithm. Prior to SDC evaluation, DWT-based denoising was applied to the noisy GW signals to improve signal quality. The resulting DI maps demonstrated that the proposed inspection framework can effectively detect and localize in-plane fibre waviness defects. It should be noted that the current investigation does not incorporate the effects of certain environmental and operational conditions, such as temperature variations and service-induced mechanical loading, which may alter guided wave velocities and potentially influence damage identification ac- curacy. Future studies will aim to integrate these factors into the simulation framework and validate the proposed methodology through experimental investigations. Additionally, further work is required to assess the sensitivity of the DI mapping approach to parameters such as defect size, orientation, and depth, as well as to evaluate its performance in the presence of multiple defects.

REFERENCES

[1] J. K. Paik, A. K. Thayamballi, and G. S. Kim, "The strength characteristics of aluminum honeycomb sandwich panels," *Thin-Walled Structures*, vol. 35, no. 3, pp. 205–231, Nov. 1999, doi: 10.1016/S0263-8231(99)00026-9.

[2] R. Talreja, "Incorporating manufacturing defects in damage and failure analysis," in Modeling Damage, Fatigue and Failure of Composite Materials, pp. 377–390, 2016, doi: 10.1016/B978-1-78242-286-0.00017-0.

[3] P. Kulkarni, K. D. Mali, and S. K. Singh, "An overview of the formation of fibre waviness and its effect on the mechanical performance of fibre reinforced polymer composites," Composites Part A: Applied Science and Manufacturing, vol. 137, p. 106013, Oct. 2020, doi: 10.1016/j.compositesa.2020.106013.

[4] H. M. Hsiao and I. M. Daniel, "Effect of fiber waviness on stiffness and strength reduction of unidirectional composites under compressive loading," Composites Science and Technology, vol. 56, no. 5, pp. 581–593, Jan. 1996, doi: 10.1016/0266-3538(96)00045-0.

[5] J. F. Mandell, D. D. Samborsky, and L. Wang, "Effects of fiber waviness on composites for wind turbine blades," in Proc. Int. SAMPE Symp. and Exhibition, pp. 2653–2666, 2003.

[6] P. Kulkarni, K. D. Mali, and S. K. Singh, "An overview of the formation of fibre waviness and its effect on the mechanical performance of fibre reinforced polymer composites," Composites Part A: Applied Science and Manufacturing, vol. 137, p. 106013, 2020.

[7] N. Chakraborty, V. T. Rathod, D. R. Mahapatra, and S. Gopalakrishnan, "Guided wave-based detection of damage in honeycomb core sandwich structures," NDT & E International, vol. 49, pp. 27–33, 2012.

[8] T. Rellinger, P. R. Underhill, T. W. Krause, and D. Wowk, "Combining eddy current, thermography and laser scanning to characterize low-velocity

impact damage in aerospace composite sandwich panels," NDT & E International, vol. 120, p. 102421, 2021.

[9] Z. Zeng, J. Wang, X. Liu, J. Lin, and Y. Dai, "Detection of fiber waviness in CFRP using eddy current method," Composite Structures, vol. 229, p. 111411, 2019.

[10] M. P. F. Sutcliffe, S. L. Lemanski, and A. E. Scott, "Measurement of fibre waviness in industrial composite components," Composites Science and Technology, vol. 72, no. 16, pp. 2016–2023, 2012.

[11] H. Fernandes, H. Zhang, C. Ibarra-Castanedo, and X. Maldague, "Fiber orientation assessment on randomly-oriented strand composites by means of infrared thermography," Composites Science and Technology, vol. 121, pp. 25–33, 2015.

[12] H. Heuer, M. H. Schulze, and N. Meyendorf, "High resolution inspection of carbon fiber materials by eddy current techniques," in Proc. 2nd Int. Symp. NDT in Aerospace, Hamburg, Germany, vol. 2, p. A3, 2010.

[13] L. Ma and M. Soleimani, "Hidden defect identification in carbon fibre reinforced polymer plates using magnetic induction tomography," Measurement Science and Technology, vol. 25, no. 5, p. 055404, 2014.

[14] C. Schmidt, C. Schultz, P. Weber, and B. Denkena, "Evaluation of eddy current testing for quality assurance and process monitoring of automated fiber placement," Composites Part B: Engineering, vol. 56, pp. 109–116, 2014.

[15] Z. Zhang, Q. Li, M. Liu, W. Yang, and Y. Ang, "Through transmission ultrasonic inspection of fiber waviness for thickness-tapered composites using ultrasound non-reciprocity: Simulation and experiment," Ultrasonics, vol. 123, p. 106716, 2022.

[16] N. Xu and Z. Zhou, "Numerical simulation and experiment for inspection of corner-shaped components using ultrasonic phased array," NDT & E International, vol. 63, pp. 28–34, 2014.

[17] Z. Zhang, M. Liu, Q. Li, and Y. Ang, "Visualized characterization of diversified defects in thick aerospace composites using ultrasonic B-scan," Composites Communications, vol. 22, p. 100435, 2020.

[18] Z. Zhang, S. Guo, Q. Li, F. Cui, A. A. Malcolm, Z. Su, and M. Liu, "Ultrasonic detection and characterization of delamination and rich resin in thick composites with waviness," Composites Science and Technology, vol. 189, p. 108016, 2020.

[19] Z. Su, L. Ye, and Y. Lu, "Guided Lamb waves for identification of damage in composite structures: A review," Journal of Sound and Vibration, vol. 295, no. 3–5, pp. 753–780, 2006.

[20] S. Sawant, S. Patil, J. Thalapil, S. Banerjee, and S. Tallur, "Temperature variation compensated damage classification and localisation in ultrasonic guided wave SHM using self-learnt features and Gaussian mixture models," Smart Materials and Structures, vol. 31, no. 5, p. 055008, 2022.

[21] S. K. Chakrapani, D. Barnard, and V. Dayal, "Detection of in-plane fiber waviness in composite laminates using guided Lamb modes," in AIP Conf. Proc., vol. 1581, no. 1, pp. 1134–1140, 2014.

[22] J. Wang, K. D. Potter, K. Hazra, and M. R. Wisnom, "Experimental fabrication and characterization of out-of-plane fiber waviness in continuous fiber-reinforced composites," Journal of Composite Materials, vol. 46, no. 17, pp. 2041–2053, 2012.

[23] M. R. Garnich and G. Karami, "Localized fiber waviness and implications for failure in unidirectional composites," Journal of Composite Materials, vol. 39, no. 14, pp. 1225–1245, 2005.

[24] H. M. Hsiao and I. M. Daniel, "Effect of fiber waviness on stiffness and strength reduction of unidirectional composites under compressive loading," Composites Science and Technology, vol. 56, no. 5, pp. 581–593, 1996.

[25] C. A. C. Leckey, K. R. Wheeler, V. N. Hafiychuk, H. Hafiychuk, and D. A. Timuçin, "Simulation of guided-wave ultrasound propagation in composite laminates: Benchmark comparisons of numerical codes and experiment," Ultrasonics, vol. 84, pp. 187–200, 2018.

[26] Q. Lei, Y. Xixi, L. Xiaodong, and Y. Shenfang, "Multiphysics simulation method of Lamb wave propagation with piezoelectric transducers under load condition," Chinese Journal of Aeronautics, vol. 32, no. 5, pp. 1071–1086, 2019.

[27] S. Sawant, S. Banerjee, and S. Tallur, "Performance evaluation of compressive sensing based lost data recovery using OMP for damage index estimation in ultrasonic SHM," Ultrasonics, vol. 115, p. 106439, 2021.

[28] M. Rautela and S. Gopalakrishnan, "Ultrasonic

guided wave based structural damage detection and localization using model assisted convolutional and recurrent neural networks," Expert Systems with Applications, vol. 167, p. 114189, 2021.

[29] S. K. Pedram, S. Fateri, L. Gan, A. Haig, and K. Thornicroft, "Split-spectrum processing technique for SNR enhancement of ultrasonic guided wave," Ultrasonics, vol. 83, pp. 48–59, 2018.

[30] S. J. Lee, N. Gandhi, J. S. Hall, J. E. Michaels, B. Xu, T. E. Michaels, and M. Ruzzene, "Baseline-free guided wave imaging via adaptive source removal," Structural Health Monitoring, vol. 11, no. 4, pp. 472–481, 2012.

[31] C. Fendzi, M. Rebillat, N. Mechbal, M. Guskov, and G. Coffignal, "A data-driven temperature compensation approach for structural health monitoring using Lamb waves," Structural Health Monitoring, vol. 15, no. 5, pp. 525–540, 2016.

[32] P. Rizzo, F. Lanza di Scalea, S. Banerjee, and A. Mal, "Ultrasonic characterization and inspection of open cell foams," Journal of Engineering *Mechanics*, vol. 131, no. 11, pp. 1200–1208, 2005.

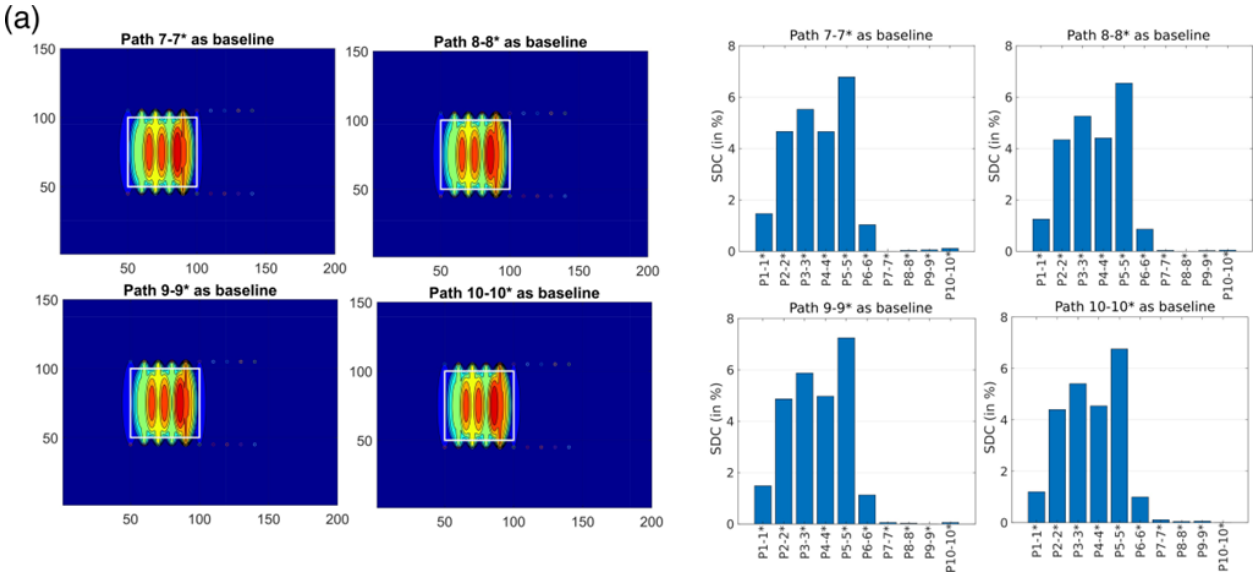

Fig. 7. SDC for each sensor path computed for FE simulated data with 20 dB added noise with in-plane fibre waviness defect present in top CFRP skin, with path P7-7*, P8-8*, P9-9* and P10-10* as baseline. The location of the actual damage is shown by the box with white edges.